

Article

Not peer-reviewed version

---

# Additive manufacturing of High Entropy Alloys: Trends, challenges and future perspectives

---

[Mainak Saha](#)\*

Posted Date: 3 October 2023

doi: 10.20944/preprints202309.2081.v1

Keywords: Additive manufacturing; compositionally complex alloys; microstructure-property correlation



Preprints.org is a free multidiscipline platform providing preprint service that is dedicated to making early versions of research outputs permanently available and citable. Preprints posted at Preprints.org appear in Web of Science, Crossref, Google Scholar, Scilit, Europe PMC.

Copyright: This is an open access article distributed under the Creative Commons Attribution License which permits unrestricted use, distribution, and reproduction in any medium, provided the original work is properly cited.

Electronic copy available at: <https://ssrn.com/abstract=4622667>

Article

# Additive Manufacturing of High Entropy Alloys: Trends, Challenges and Future Perspectives

Mainak Saha <sup>1,2</sup>

<sup>1</sup> Department of Metallurgical and Materials Engineering, Indian Institute of Technology, Madras, Chennai-600036 ORCID: 0000-0001-8979-457x; mainaksaha1995@gmail.com, Phone number: +918017457062

<sup>2</sup> Department of Metallurgical and Materials Engineering, National Institute of Technology, Durgapur-713209

**Abstract:** The recent decade has witnessed the evolution of a novel paradigm of alloying which is based on utilising multiple elements to design compositionally complex alloys also known as high entropy alloys (HEAs). Conventional manufacturing of HEAs has a number of drawbacks, especially in terms of mechanical properties and design complexities. This has been addressed by additive manufacturing (AM), which has not only led to the fabrication of complex-shaped HEA components but has also enabled both ex-situ and in-situ tailoring of alloy microstructures. Considering the increasing interest in AM-based fabrication of HEAs in the last ten years, the present chapter is aimed at highlighting the present status and challenges in the avenue of AM of HEAs. This has been followed by a discussion on the recent trends in the avenue of AM-based fabrication of HEAs from the viewpoints of (i) microstructure evolution and mechanical properties, and (ii) alloy fabrication techniques. The chapter ends with a discussion on the future prospects in the aforementioned avenue.

**Keywords:** additive manufacturing; compositionally complex alloys; microstructure-property correlation

## 1. Introduction

In recent times, there has been a huge number of investigations aimed at fabricating high-entropy alloys (HEAs) using additive manufacturing (AM) [1], [2]. This may be primarily attributed to the two factors: (i) microstructural optimisation, and (ii) enhanced mechanical properties [2], [3]. The former is associated with defect density along with low cost (of production) whereas the latter is mainly a subset of the former factor [4]–[8]. In other words, the microstructure plays a crucial role in influencing the mechanical response of AM-based HEAs [4], [9]–[13]. It has recently been reported that AM-based HEAs possess a higher overall toughness (including yield strength and ductility) when compared to those of the bulk counterparts [14]–[17]. In addition, AM has provided a wide range of opportunities towards manufacturing HEA components with (i) high geometrical complexities and (ii) in-situ tailoring of microstructures [18]–[26]. The fabrication technique employed during AM highly influences the latter. For instance, the fine-grained microstructure evolved during rapid solidification has been reported to undergo hot isostatic pressing (HIP), for further enhancement of mechanical properties through removal of fabrication defects and residual stresses in AM-based HEAs [27]–[31]. Moreover, the high cooling rates associated with AM-based techniques may be used to avoid undesired phase transformations and chemically homogenise the HEAs by restricting diffusion [32].

The high heating and cooling rates associated with AM-based fabrication techniques lead to fine-grained microstructures with enhanced mechanical properties [31]. More specifically, the non-equilibrium nature of the AM-based fabrication techniques has also been reported to suppress the formation of intermetallic compounds during solidification [31]. In the context of beam (laser and electron beam)-based AM techniques, heat transfer is highly anisotropic and leads to the formation of textured columnar grains along the build direction (in the as-fabricated condition of the alloy) [31]. In a series of recent investigations, a number of techniques have been devised for controlling the

microstructural features such as grain morphology, texture, residual stresses, and residual stresses (during solidification) [11], [31]. Two of the most common techniques to control the aforementioned features include (i) laser power and (ii) scan strategy [31]. From the viewpoint of microstructural features and mechanical properties, the recent developments in the avenue of AM-based HEAs include the development of interstitial HEAs, core-shell structured HEAs, and HEA composites. From the viewpoint of HEA fabrication, development of non-beam AM techniques is a major breakthrough in the aforementioned avenue [31]. Considering the expanding interests of the alloy design community in the avenue of AM-based fabrication of HEAs (in the last few years), the present chapter begins with a brief discussion on the present status and challenges in the area of AM-based HEAs. This has been followed by a discussion on the recent trends in AM of HEAs from two different viewpoints, viz. (i) microstructural features and mechanical properties, and (ii) alloy fabrication. Moreover, future perspectives in the avenue of AM of HEAs have also been highlighted.

## 2. Present status and challenges in the avenue of AM-based HEAs

Direct laser deposition (DLD) and electron beam melting (EBM) are the two most commonly used AM techniques for the fabrication of HEAs [32]. However, there has been a limited number of investigations on the selective laser manufacturing (SLM) of HEAs [32]. In contrast to EBM and SLM techniques, which require pre-alloyed powders, DLD uses elemental powders to fabricate HEAs and also enables tailoring of HEA compositions [32]. However, SLM and EBM have much finer beam diameter and can tune the microstructure at higher resolution than DLD [32]. Joseph et al. [33] have used DLD technique to fabricate  $Al_xCoCrFeNi$  HEA with different mole fractions of Al ( $x = 0.3, 0.6,$  and  $0.85$ ). It was reported that a variation in Al content leads to three different microstructures, viz. FCC, FCC/BCC, and BCC. For instance, DLD-based  $Al_{0.6}CoCrFeNi$  HEA shows a Widmanstatten microstructure at room temperature [33]. A comparison of the DLD microstructure (of  $Al_{0.6}CoCrFeNi$ ) with that of conventional arc melted microstructure (**Fig. 1**) shows that there is no appreciable difference in terms of microstructural features in both FCC and BCC phases [33]. However, for the case of a dual-phase FCC + BCC microstructure, significant differences were observed between DLD and arc melted microstructures [33]. This was attributed to the (i) higher cooling rates and (ii) larger thermal gradient in the melt pool for DLD as compared to that for conventional arc melting [33].

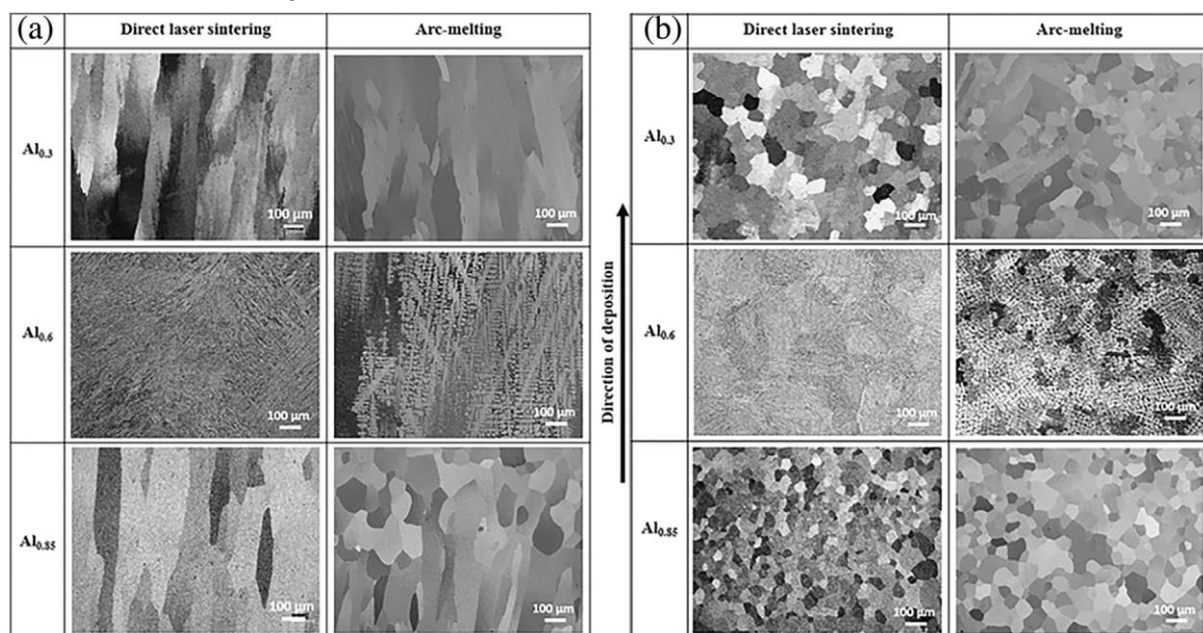


**Figure 1.** DLD-based and arc-melted  $Al_xCoCrFeNi$  HEA: (a) perpendicular to the direction of solidification, and (b) normal to the area of cross-section [33].

Sistla et al. [34] have studied the influence of Al/Ni ratio on the microstructure evolution and phase stability in DLD-based  $\text{Al}_x\text{FeCoCrNi}_{2-x}$  HEA. It was observed that a decrease in the Al/Ni ratio leads to a transition from BCC (lattice parameter= 0.288 nm) to FCC solid solution (lattice parameter= 0.357 nm) [34]. Ordering and spinodal decomposition in these alloys (during cooling) were attributed to lattice strain caused by Al [34]. In addition, as shown in **Fig. 2**, the microstructure as reported to undergo a transition from dendritic to equiaxed morphology [34]. Ocelik et al. [35] have studied the influence of laser processing parameters and that of Al content on the microstructure evolution of AlCoCrFeNi equiatomic HEA. It was reported that high cooling rates lead to a high probability towards formation of BCC phase [35]. Moreover, it was also highlighted that the efficiency of DLD technique depends on a number of process parameters which include rate of powder in-take, powder melting temperature, traveling speed, and power density of laser beam [35]. This study showed that it is feasible to fabricate HEAs via in situ alloying during DLD [35]. Dobbstein et al. [36] have used DLD technique to fabricate MoNbTaW refractory HEAs (RHEAs) using pre-mixed powders. Based on this work, it was highlighted that in-situ alloying during DLD may be used to fabricate HEAs [36]. This study demonstrated that it is possible to control the process parameters (involved in fabrication) by fine-tuning the HEA composition [36]. In the context of RHEA fabrication, a point worth noting is that all refractory metals are highly sensitive to oxidation [36].

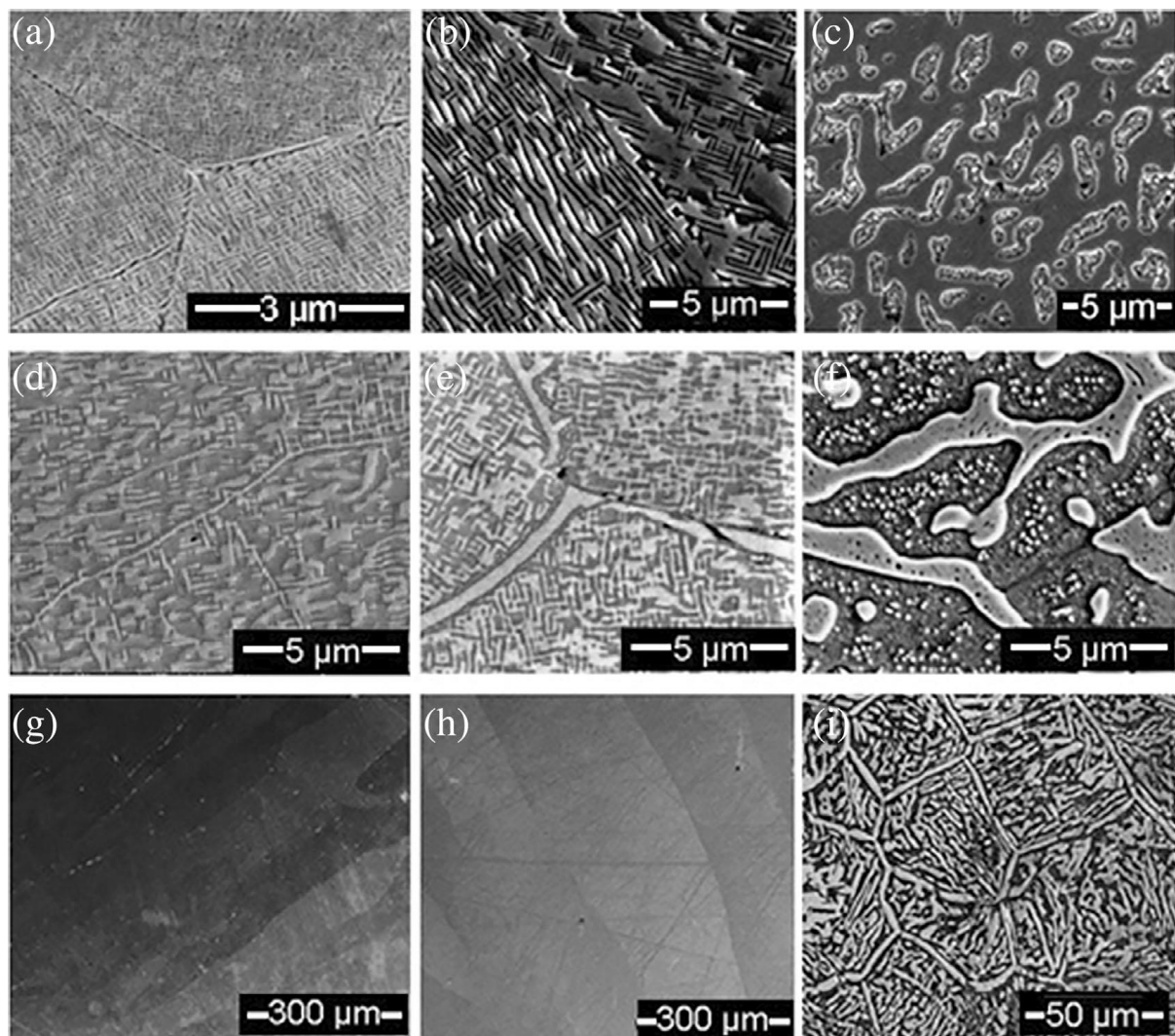


**Figure 2.** DLD-based AlCoCrFeNi HEA: (a) Equiaxed grains with modulated precipitates, (b) coarse modulated structures in the as-quenched condition, (c) Fe–Cr rich precipitates in the B2 (ordered BCC) matrix in annealed condition, (d) Fe–Cr rich precipitates in Ni–Al rich matrix deposited in pulsed mode, (e) Grain boundaries (GBs) in coarse microstructure in as-quenched condition, (f)

Coarse Fe–Cr rich precipitates formed due to a high rate of diffusion of constituent elements (Al, Co, Cr, Fe, and Ni) during annealing; DLD-based  $\text{Al}_{0.3}\text{CoCrFeNi}_{1.7}$  HEA: **(g)** columnar grain structure in as-fabricated condition, **(h)** columnar grain structure after quenching, and **(i)** equiaxed grains with coarse Al–Ni rich precipitates (coarsened due to annealing) [34].

EBM has been reported to ensure chemical homogeneity of the fabricated HEAs by using pre-alloyed HEA powders [32]. This is in contrast to DLD which uses elemental powders for fabricating HEAs [32]. as using pre-alloyed powders can to some extent ensure the chemical homogeneity in the fabricated alloys. In the context of EBM-based AlCoCrFeNi HEAs, Fujieda et al. [37] have reported that the fabricated alloy has a dual-phase FCC + BCC microstructure (evolved during preheating) whereas the raw powders had a single-phase BCC structure (**Fig. 3(a)**). BCC grains in EBM-based HEA were observed to be oriented along the build direction (BD) (**Fig. 3(b)**) [37]. Moreover, the EBM-based HEA was reported to exhibit a fine-grained microstructure in contrast to the specimen prepared by casting (**Fig. 3(b)**) [37]. This was attributed to the high cooling rates followed during EBM [37]. Both Fe and Co were observed to segregate at grain boundaries (GBs) in EBM as well as cast specimens [37]. It is also worth mentioning that the bottom part of the fabricated HEA component had a significantly higher fraction of equiaxed FCC grains when compared to the top portion of the component [37]. This was attributed to the longer preheating process which led to the transition from BCC to FCC crystal structure [37]. In the context of AlCoCrFeNi HEA, Shiratori et al. [38] have reported a microstructure comprising of nano-lamellae of BCC and B2 phases. The FCC phases were observed along the GBs of the BCC/B2 phases [38]. This was attributed to the intrinsic preheating followed during EBM [38]. In addition, BCC/B2 grains were observed to be elongated along BD on both the top and bottom parts of EBM-based specimen both of the top and bottom parts of the EBM specimens [38].



**Figure 3.** AlCoCrFeNi HEA: (a) X-Ray Diffraction (XRD) patterns of the EBM-based (red), as-cast specimen (blue) and the gas-atomised powders (green), (b) Electron backscatter diffraction (EBSD)-based Inverse pole figure (IPF) maps (left) and phase distribution maps (right) of the top and bottom portions EBM-based specimens [39].

A similarity was observed in terms of the microstructure of top portion of EBM-based specimen and cast specimens [38]. On the other hand, microstructural coarsening was observed in the bottom part where the volume fraction of FCC grains was higher than that of the BCC grains. In addition, Al-Ni and Cr-Fe rich phases were also observed on the top portion of EBM-based specimen. Fujieda et al. [40] have fabricated CoCrFeNiTi HEA using Selective EBM (SEBM) technique. In the case of SEBM-based specimen, Ni<sub>3</sub>Ti precipitates (with basketweave morphology) were observed in the FCC matrix [40]. On the other hand, both Ni<sub>3</sub>Ti and (Cr<sub>11</sub>Fe<sub>13</sub>Ni<sub>4</sub>)Mo<sub>3</sub> intermetallic phases were detected in the cast HEA (Fig. 4(a)) [40]. Clustering of both Ni and Ti elements was observed in the SEBM-based specimens, in as-fabricated condition [40]. In addition, it was reported that Ni<sub>3</sub>Ti precipitates completely disappear after solution-treatment (Fig. 4(b-d)). It is also noteworthy to mention that fine ordered phases (enriched with Ni and Ti and with an average diameter of ~40 nm) were observed in the FCC matrix (Fig. 4(b-d)) [40]. The formation of this phase was attributed to the spinodal decomposition [40]. Brif et al. [41] have fabricated equiatomic FeCoCrNi HEA with a single-phase FCC structure through SLM of pre-alloyed powders. Based on this work, it was demonstrated that post-heat treatment is necessary for chemical homogenisation of SLM-based HEA specimens [41].

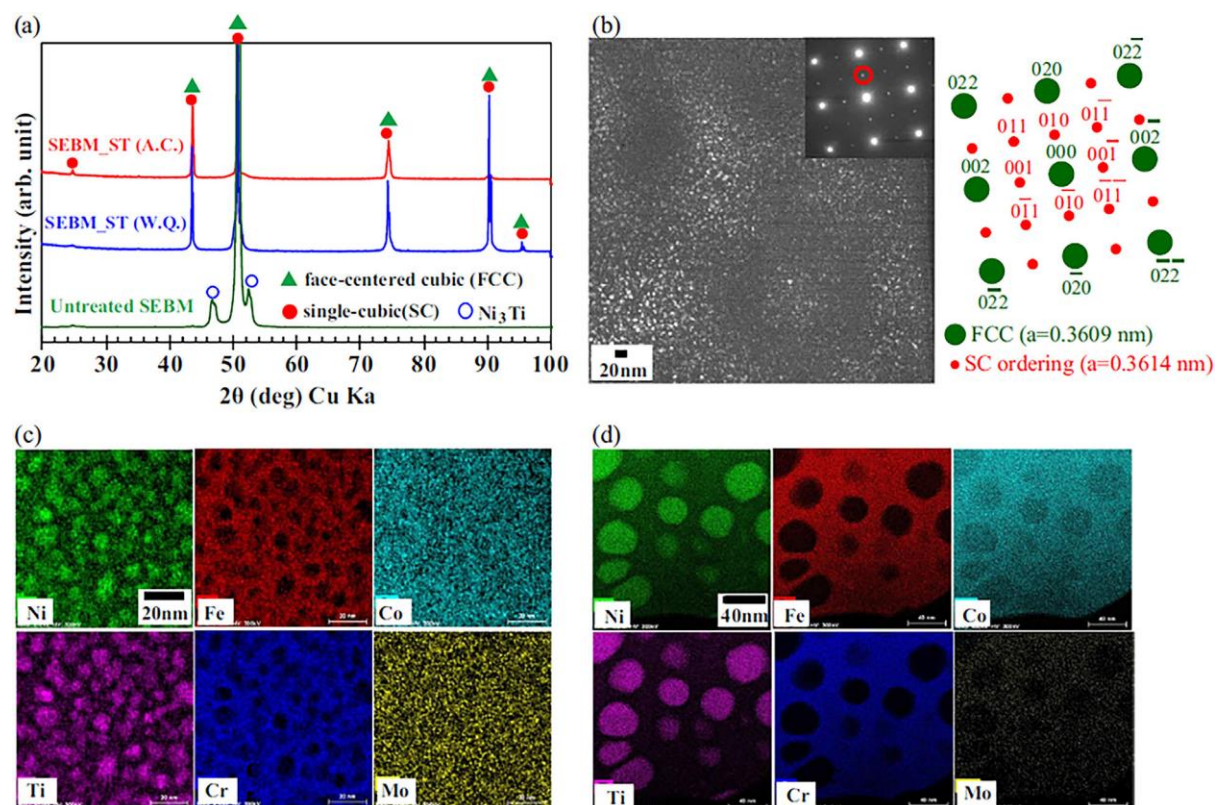


**Figure 4.** SEBM-based CoCrFeNiTi HEA: (a) XRD patterns in the as-fabricated and solution-treated conditions, (b) Transmission Electron Microscopy (TEM)-dark-field (DF) image and corresponding Selected Area Diffraction Pattern (SADP) after solutionising (inset), (c) Scanning Transmission Electron Microscope (STEM)-Energy Dispersive X-Ray Spectroscopy (STEM-EDS) elemental maps with elemental mappings for specimens water-quenched after solutionising, and (d) STEM-EDS based elemental maps after normalising (in post solution treated condition) [42].

### 3. Trends in AM-based fabrication of HEAs

### 3.1. From the viewpoint of microstructural features and mechanical properties

#### 3.1.1. Design of interstitial HEAs

Addition of an interstitial element such as carbon (C) has been reported to simultaneously activate twinning-induced plasticity (TWIP) and transformation-induced plasticity (TRIP) mechanisms in a metastable  $\text{Fe}_{49.5}\text{Mn}_{30}\text{Co}_{10}\text{Cr}_{10}\text{C}_{0.5}$  HEA [43]–[45]. Zhu et al. [43] have reported the feasibility of fabricating dense C-added  $\text{Fe}_{49.5}\text{Mn}_{30}\text{Co}_{10}\text{Cr}_{10}\text{C}_{0.5}$  interstitial HEAs using SLM technique. It was highlighted that the overall toughness of SLM-based specimens were significantly higher than those of the conventionally cast specimens with coarse-grained microstructures [43]. Planar slip bands, and deformation twins were observed during the early stages of deformation in SLMed HEA [43]. However, with increase in the extent of deformation (to ~12%), intersection of slip bands with profuse stacking faults (SFs) was observed [43]. These deformation features were reported to be promote work-hardening leading to an overall enhancement in both strength and ductility of SLMed HEA [43].

Park et al. [46] have reported that addition of ~ 0.2 wt.% C leads to a significant improvement in the mechanical properties of SLM-based  $\text{CoCrFeMnNi}$  equiatomic HEA. Two laser scanning speeds were used, viz. 200 and 600  $\text{mms}^{-1}$  [46]. Enhancement in mechanical properties was attributed to a number of factors, viz. solid solution strengthening, formation of dislocation pile-ups, and grain refinement [46]. Addition of C was interestingly observed to promote the formation of  $\text{Cr}_{23}\text{C}_6$ ,  $\text{MnO}$  and  $\text{MnS}$  in the form of nanoprecipitates [46]. In the case of 200  $\text{mms}^{-1}$ , it was observed that slow laser scan speed leads to segregation of Mn and Ni segregation at cellular networks [46]. Segregation of these elements was reported to induce plastic strains at the interface, leading to the pile-up of geometrically necessary dislocations (GNDs) in the interfacial region [46]. The back-stresses produced due to this pile-up leads to back-stresses which contribute to the excellent mechanical properties of  $(\text{CoCrFeMnNi})_{99}\text{C}_1$  HEA [46]. In the context of SLM-based  $\text{FeCoCrNiC}_{0.05}$  HEA with fine-grained FCC microstructure comprising of cellular and columnar subgrains, Zhou et al. [47] have reported that the mechanical properties of the alloy are largely dependent on the laser power and travelling speed. Precipitation of nano  $\text{M}_{23}\text{C}_6$  carbides was obtained at GBs and dislocation networks. In addition, a number of defects such as nanotwins, SFs, and sessile Lomer locks, were also observed in the microstructure of the aforementioned alloy [47]. The overall elongation of C-doped SLM-based samples was reported to be significantly lower than those reported for non C-containing SLM-based specimens and C-containing cast specimens [47]. Song et al. [48] have doped Nitrogen (N) in SLM-based  $\text{CoCrFeNi}$  HEA. A hierarchical microstructure comprising of low-angle (or subgrain) boundaries, and dislocation networks was obtained [48]. Besides, N was reported to induce strengthening through grain size refinement [48].

#### 3.1.2. Core-shell structure

In the context of AM-based HEA, Zhang et al. [49] have used liquid phase separation technique to demonstrate the formation of core-shell structure during solidification (of the alloy). It was reported that the microstructure changes from dendritic to a core-shell structure through liquid phase decomposition. This decomposition was attributed to the addition of 1 wt.%  $\text{Y}_2\text{O}_3$  in the form of nanoparticles during laser cladding of  $\text{AlCoCrCuFeNiSi}_{0.5}$  HEA [49]. However, no such decomposition was observed in the absence of  $\text{Y}_2\text{O}_3$ .  $\text{Y}_2\text{O}_3$  nanoparticles was reported to be a catalyst for liquid phase decomposition [49]. Addition of  $\text{Y}_2\text{O}_3$  nanoparticles was reported to promote the formation of Cu-rich FCC phase in addition to the existing FCC+BCC dual-phase microstructure [49]. Cu-rich FCC phase was observed to be present only in the core. Moreover, a uniform distribution of core-shell structures was reported in the BCC matrix phase [49]. Formation of core-shell structure was also reported in laser clad  $\text{CoCrFeNiAl}_x\text{Cu}_{0.7}\text{Si}_{0.1}\text{B}_y$  ( $x=0.3$  and  $2.3$ ,  $0.3 \leq y \leq 0.6$ ) HEA coatings [50]. However, till date, there is no report on the mechanical properties of these coatings.

#### 3.1.3. HEA-based composites

At present, HEA-based composites (HEACs) comprising of borides, nitrides, carbides and oxides (added both ex-situ and in-situ during AM-based fabrication) have been introduced for the purpose of tailoring the microstructure of AM-based HEAs [51], [52]. The first report in this avenue was obtained from Li et al. [52] where DLD technique was used to deposit three compositions, viz. FeCoCrAlCu, 97.5(FeCoCrAlCu)-2.5(YPSZ) (YPSZ: Ytria partially stabilised zirconia) and 90.5(FeCoCrAlCu)-2.5(YPSZ)-7(SiB<sub>2</sub>) (wt %) on TC17 Ti alloy. Moreover, formation of AlCu<sub>2</sub>Zr ultra-nanocrystals (UNs) was observed and attributed to the high magnitude of enthalpies of mixing between Cu and other elements in FeCoCrAlCu [52]. Amar et al. [51] have reported the influence of carbides, namely TiC and WC on the microstructure evolution and mechanical properties of equiatomic CoCrFeMnNi. CoCrFeMnNi-5 wt % TiC composite was reported to possess an ultimate tensile strength (UTS) of ~723 MPa with an overall ductility of ~32% [51]. On the other hand, CoCrFeMnNi-5 wt %WC composite was reported to show a comparatively higher UTS (~800 MPa) with a slightly higher elongation (~37%) [51]. Enhancement in mechanical properties was attributed to the hindered propagation of slip bands due to the presence of TiC (in the form of second phase for TiC-reinforced composite) or Cr<sub>23</sub>C<sub>6</sub> precipitate [51]. Similarly, Li et al. [53] have reported the fabrication of CoCrFeMnNi-TiN HEA using SLM. of pre-alloyed CoCrFeMnNi gas-atomized powder and TiN nanoparticles were used as the starting materials for this fabrication. Strengthening of the alloy was attributed to pinning caused by the presence of uniformly dispersed TiN nanoparticles. UTS and overall elongation of the alloy was reported to be ~1036 MPa and 12% respectively [53]. In addition, Li et al. [53] have fabricated Fe<sub>43.7</sub>Co<sub>7.3</sub>Cr<sub>14.7</sub>Mo<sub>12.6</sub>C<sub>15.5</sub>B<sub>4.3</sub>Y<sub>1.9</sub> metallic glass reinforced CoCrFeMnNi HEAC using SLM. These composites were reported to possess UTS in the range of ~916–1517 MPa [53]. UTS of these composites was reported to be influenced by the volume fraction of metallic glass [53]. Jiang et al. [54] and Chen et al. [55] have reported the laser cladding-based fabrication of AlCoCrFeNiTi-CeO<sub>2</sub> and AlCoCrFeNiTi-TiC HEAC coatings respectively. Chen et al. [55] have added C and B to fabricate self-generated TiC particle reinforced AlCoCrFeNiTi HEAC coating on #45 steel. Self-generation of TiC particles was reported with an increase in the fraction of B and C (from 2 to 4 wt.%) [55]. Moreover, B and C were reported to cause a transition (in the crystal structure of the coatings) from FCC to BCC [50], [55]. It was further reported that the mechanical properties of laser-cladded AlCoCrFeNiTi-1 wt. % CeO<sub>2</sub> HEAC were enhanced when compared with those of AlCoCrFeNiTi HEA [55].

### 3.2. From the viewpoint of HEA fabrication

#### 3.2.1. Non-beam AM techniques

One of the most recent developments in the field of AM is the development of powder-based liquid ink AM techniques. The most common technique using this approach is 3D ink extrusion which involves room temperature printing of an ink-containing blend of precursor powders into a green structure. This is followed by a number of isothermal thermochemical processing steps for transformation of the green component into a sintered one [56]. Recently, Kenel et al. [56] have used this technique to fabricate micro-lattices of CoCrFeNi quaternary HEA. This technique has been reported to overcome segregation-based inhomogeneities, thereby reducing the residual stresses in the printed component [56]. In the work of Kenel et al. [56], the printable ink for 3D ink extrusion AM technique was developed by blending a number of oxide nanopowders, namely Fe<sub>2</sub>O<sub>3</sub>, NiO, Co<sub>3</sub>O<sub>4</sub> and Cr<sub>2</sub>O with a polymeric mixture [56]. This was followed by the extrusion of the ink into 200 nm micro-lattices [56]. These micro-lattices were subsequently made to undergo co-reduction, interdiffusion and sintering in H<sub>2</sub> atmosphere [56]. The CoCrFeNi HEA was prepared by reduction and metal inter-diffusion of the sintered product [56]. This alloy was reported to show excellent sub-zero temperature mechanical properties (including UTS~864 MPa and elongation~ 37.6% at 137 K) [56]. Surjadi et al. [57] have fabricated equiatomic CoCrFeMnNi HEA-coated 3D polymeric core-shell micro-lattices (with high specific compressive strength of ~0.018MPa kg<sup>-1</sup>m<sup>3</sup>) using stereolithography (for the fabrication of polymeric scaffold) and RF magnetron sputtering techniques (for coating CoCrFeMnNi HEA thin film onto the scaffold).

#### 4. AM of HEAs: future perspectives

Both powder-bed and powder-flow based AM techniques involve a series of unique complex thermomechanical and rapid solidification techniques [32]. These involve cyclic heating and cooling of the fabricated specimens [1]. This sets AM-based techniques apart from conventional fabrication techniques. In the context of AM for HEAs, the present state of research is focussed mainly on utilizing HEA powders produced by gas-atomization technique [2]. As highlighted by Li [32], not all HEAs can be fabricated using AM. This necessitates extensive investigations on the (i) process parameters of different AM-based techniques and (ii) composition and microstructure of HEAs. For instance, a number of parameters such as laser velocity, laser power, laser absorptivity, fluidity (of the metal), and powder melting temperature need to be considered during SLM of HEAs [3], [9]. In addition, the resistance to crack formation of the HEAs and the ability to overcome high residual stresses associated with high thermal gradients (during AM-based fabrication techniques) must be considered for the design of AM-based HEAs [32].

The other challenge to be overcome is to establish a systematic structure-property correlation in AM-based HEAs [32]. For instance, the influence of laser parameters such as laser power and density on the chemical homogeneity of the melt pool in HEAs is still not fully understood till date [32]. In addition, the role of interstitial atoms such as B, N, and C and contaminants (for example, oxygen) on the phase evolution and mechanical properties of AM-based HEAs is not completely clear [32]. Besides, not much is known about the solidification process (during AM) and its associated influence on the residual stress [33]. In the context of mechanical properties, creep deformation behaviour and fatigue response of AM-based HEAs, are the areas where limited information exists [31], [37]. Besides, the poor surface quality of AM-based HEAs necessitates extensive surface machining. Altogether, these are the major avenues which show enormous potential for future experimental and theoretical investigations [58]. In this context, it is important to highlight that laser shock peening (LSP) has already been reported to show a tremendous potential towards improving mechanical properties (through the reduction of porosities) [31]. However, extensive microstructural investigations are required to understand the compatibility of different HEA systems with LSP before commercialising the process [31]. Such investigations are also necessary to understand the mechanism(s) and sequence of precipitation hardening in age-hardenable AM-based HEA systems [31].

From a broader viewpoint, AM-based fabrication techniques for HEAs are currently based on a trial-and-error principle and is still at its very early stage, which is highly time-consuming and also costly [59]. Besides, characterisation of melt pool during AM involves a very small interaction volume between the source (energy source) and powder particles [60]. This may be attributed to very high heating and cooling rates associated with AM-based fabrication methods [60]. Hence, there is a very limited information on the heating and cooling processes at different regions of the melt pool during AM-based fabrication techniques [34]. Moreover, owing to the non-equilibrium nature of AM-based fabrication techniques, a number of process and material parameters influence the fabrication process [5], [6], [33], [61], [62]. Understanding these parameters experimentally, is a highly challenging. In order to overcome this issue, experimental observations need to be coupled with appropriate computation-based modelling approach which include integrated computational materials engineering (ICME), machine learning, and artificial intelligence. To the best of the author's knowledge, no applications of AM-based HEAs have been reported till date. Currently, hybrid AM techniques are being developed with high manufacturing capacity at a low operational cost. Nevertheless, such developments may be expected to render AM-based fabrication as suitable options for large-scale economic manufacturing of HEAs.

#### 5. Conclusions

The chapter presents an overview of the current state of research in the avenue of AM of HEAs with a special focus on (i) structure-property correlation, and (ii) fabrication techniques. At present, fabrication of fabricating complex geometric HEAs using conventional fabrication techniques, needs further investigations (more particularly, microstructure-based investigations). In order to utilise the tremendous potentials offered by AM-based fabrication of HEAs, not only novel HEAs need to be

developed but also new fabrication techniques (such as 3D ink extrusion technique, as discussed in section 3.2.1) for fabricating structurally homogeneous HEAs at low cost need to be designed. Besides, there is a huge requirement of coupling the experimental observations with appropriate computation-based modelling approaches. It is also worth mentioning that novel compositions (of the inks) and sintering mechanisms during 3D ink extrusion needs to be further investigated.

## References

1. S. Luo, P. Gao, H. Yu, J. Yang, Z. Wang, and X. Zeng, "Selective laser melting of an equiatomic AlCrCuFeNi high-entropy alloy: Processability, non-equilibrium microstructure and mechanical behavior," *J Alloys Compd*, vol. 771, pp. 387–397, Jan. 2019.
2. P. Wang *et al.*, "Additively manufactured CoCrFeNiMn high-entropy alloy via pre-alloyed powder," *Mater Des*, vol. 168, Apr. 2019.
3. H. Dobbelsstein, E. L. Gurevich, E. P. George, A. Ostendorf, and G. Laplanche, "Laser metal deposition of compositionally graded TiZrNbTa refractory high-entropy alloys using elemental powder blends," *Addit Manuf*, vol. 25, pp. 252–262, Jan. 2019.
4. N. Li *et al.*, "Progress in additive manufacturing on new materials: A review," *J Mater Sci Technol*, vol. 35, no. 2, pp. 242–269, Feb. 2019.
5. M. Saha, "3D printing of nanoceramics: Present status and future perspectives," Sep. 2022, doi: 10.48550/arxiv.2210.06948.
6. M. Saha, "On the advanced microstructural characterisation of additively manufactured alumina-zirconia based eutectic ceramics: Overview and outlook," Dec. 2022, doi: 10.26434/CHEMRXIV-2022-84LD6.
7. M. Saha and M. Mallik, "Additive Manufacturing and Characterisation of Biomedical Materials," *Advanced Materials for Biomechanical Applications*, pp. 29–57, May 2022, doi: 10.1201/9781003286806-3.
8. M. Saha and M. Mallik, "Additive manufacturing of ceramics and cermets: present status and future perspectives," *Sādhanā* 2021 46:3, vol. 46, no. 3, pp. 1–35, Aug. 2021, doi: 10.1007/S12046-021-01685-2.
9. B. Gwalani, V. Soni, O. A. Waseem, S. A. Mantri, and R. Banerjee, "Laser additive manufacturing of compositionally graded AlCrFeMoV<sub>x</sub> (x = 0 to 1) high-entropy alloy system," *Opt Laser Technol*, vol. 113, pp. 330–337, May 2019.
10. M. Saha, "A brief discussion on the tensile creep deformation behaviour of wrought single-phase  $\gamma$ -TiAl," *Mater Today Proc*, Jan. 2021, doi: 10.1016/j.matpr.2020.11.189.
11. M. Saha, "Understanding the role of Al<sub>2</sub>O<sub>3</sub> formed during isothermal oxidation in a dual phase AlCoCrFeNi<sub>2.1</sub> Eutectic High-Entropy Alloy," *Journal of Materials NanoScience*, vol. 7, no. 2, pp. 68–72, Nov. 2020, [Online]. Available: <http://thesciencein.org/journal/index.php/jmns/article/view/119>
12. M. Saha and M. Mallik, "3D printing of nanoceramics for biomedical applications," *Advanced Ceramic Coatings for Biomedical Applications*, pp. 111–135, Jan. 2023, doi: 10.1016/B978-0-323-99626-6.00002-0.
13. M. Saha and M. Mallik, "Metal-based conductive nano-inks: synthesis and characterization techniques," *Smart Multifunctional Nano-Inks*, pp. 27–52, Jan. 2023, doi: 10.1016/B978-0-323-91145-0.00003-7.
14. H. Diao, X. Xie, F. Sun, K. A. Dahmen, and P. K. Liaw, "Mechanical properties of high-entropy alloys," *High-Entropy Alloys: Fundamentals and Applications*, pp. 181–236, Jan. 2016, doi: 10.1007/978-3-319-27013-5\_6.
15. A. Amar *et al.*, "Additive manufacturing of high-strength CrMnFeCoNi-based High Entropy Alloys with TiC addition," *Intermetallics (Barking)*, vol. 109, pp. 162–166, Jun. 2019.
16. S. Chen, X. Chen, L. Wang, J. Liang, and C. Liu, "Laser cladding FeCrCoNiTiAl high entropy alloy coatings reinforced with self-generated TiC particles," *J Laser Appl*, vol. 29, no. 1, p. 012004, Feb. 2017, doi: 10.2351/1.4966052.
17. Y. He, J. Zhang, H. Zhang, and G. Song, "Effects of different levels of boron on microstructure and hardness of CoCrFeNiAl x Cu 0.7 Si 0.1 B y high-entropy alloy coatings by laser cladding," *Coatings*, vol. 7, no. 1, Jan. 2017, doi: 10.3390/COATINGS7010007.
18. V. Ocelík, N. Janssen, S. N. Smith, and J. T. M. de Hosson, "Additive Manufacturing of High-Entropy Alloys by Laser Processing," *JOM*, vol. 68, no. 7, pp. 1810–1818, Jul. 2016, doi: 10.1007/S11837-016-1888-Z.
19. C. Zhang, G. J. Chen, and P. Q. Dai, "Evolution of the microstructure and properties of laser-clad FeCrNiCoB<sub>x</sub> high-entropy alloy coatings," *Materials Science and Technology (United Kingdom)*, vol. 32, no. 16, pp. 1666–1672, Nov. 2016, doi: 10.1080/02670836.2015.1138035.
20. M. Saha, "Grain boundary segregation in steels: Towards engineering the design of internal interfaces," Feb. 2022, doi: 10.48550/arxiv.2202.12971.

21. M. Saha, "New frontiers in characterising ZrB<sub>2</sub>-MoSi<sub>2</sub> ultra-high temperature ceramics," Feb. 2022, doi: 10.48550/arxiv.2202.11162.
22. M. Saha, "α-TiAl alloy: revisiting tensile creep deformation behaviour and creep life at 832 °C," *Advances in Materials and Processing Technologies*, 2021, doi: 10.1080/2374068X.2021.1949175.
23. M. Saha, "Fly ash composites: A review," Feb. 2022, doi: 10.48550/arxiv.2202.11167.
24. M. Saha and M. Mallik, "Surface engineering of nanomaterials: Processing and applications," *Surface Engineering*, pp. 95–119, Dec. 2022, doi: 10.1201/9781003319375-4.
25. M. Saha *et al.*, "An Insight Into Cyclic Oxidation behavior of ZrB<sub>2</sub>-20 Vol.% MoSi<sub>2</sub> Based Ultrahigh Temperature Ceramic Matrix Composite," *Modern Manufacturing Systems*, pp. 149–163, Dec. 2022, doi: 10.1201/9781003284024-13.
26. M. Mallik and M. Saha, "Carbon-Based Nanocomposites: Processing, Electronic Properties and Applications," Springer, Singapore, 2021, pp. 97–122. doi: 10.1007/978-981-16-1052-3\_5.
27. M. Zhang, W. Zhang, F. Liu, Y. Peng, S. Hu, and Y. Liu, "Effect of binding and dispersion behavior of high-entropy alloy (HEA) powders on the microstructure and mechanical properties in a novel HEA/diamond composite," *Entropy*, vol. 20, no. 12, Dec. 2018, doi: 10.3390/E20120924.
28. J. Kim, A. Wakai, and A. Moridi, "Materials and manufacturing renaissance: Additive manufacturing of high-entropy alloys," *J Mater Res*, vol. 35, no. 15, pp. 1963–1983, Aug. 2020, doi: 10.1557/JMR.2020.140.
29. S. Chen, Y. Tong, and P. K. Liaw, "Additive manufacturing of high-entropy alloys: A review," *Entropy*, vol. 20, no. 12, Dec. 2018, doi: 10.3390/E20120937.
30. X. Li, "Additive Manufacturing of Advanced Multi-Component Alloys: Bulk Metallic Glasses and High Entropy Alloys," *Adv Eng Mater*, vol. 20, no. 5, May 2018, doi: 10.1002/ADEM.201700874.
31. A. Ostovari Moghaddam, N. A. Shaburova, M. N. Samodurova, A. Abdollahzadeh, and E. A. Trofimov, "Additive manufacturing of high entropy alloys: A practical review," *J Mater Sci Technol*, vol. 77, pp. 131–162, Jun. 2021, doi: 10.1016/J.JMST.2020.11.029.
32. X. Li, "Additive Manufacturing of Advanced Multi-Component Alloys: Bulk Metallic Glasses and High Entropy Alloys," *Adv Eng Mater*, vol. 20, no. 5, p. 1700874, May 2018, doi: 10.1002/ADEM.201700874.
33. J. Joseph, T. Jarvis, X. Wu, N. Stanford, P. Hodgson, and D. M. Fabijanic, "Comparative study of the microstructures and mechanical properties of direct laser fabricated and arc-melted Al<sub>x</sub>CoCrFeNi high entropy alloys," *Materials Science and Engineering: A*, vol. 633, pp. 184–193, May 2015, doi: 10.1016/J.MSEA.2015.02.072.
34. H. R. Sistla, J. W. Newkirk, and F. Frank Liou, "Effect of Al/Ni ratio, heat treatment on phase transformations and microstructure of Al<sub>x</sub>FeCoCrNi<sub>2-x</sub> (x = 0.3, 1) high entropy alloys," *Mater Des*, vol. 81, pp. 113–121, Sep. 2015, doi: 10.1016/J.MATDES.2015.05.027.
35. V. Ocelík, N. Janssen, S. N. Smith, and J. Th. M. de Hosson, "Additive Manufacturing of High-Entropy Alloys by Laser Processing," *JOM* 2016 68:7, vol. 68, no. 7, pp. 1810–1818, Apr. 2016, doi: 10.1007/S11837-016-1888-Z.
36. H. Dobbstein, M. Thiele, E. L. Gurevich, E. P. George, and A. Ostendorf, "Direct Metal Deposition of Refractory High Entropy Alloy MoNbTaW," *Phys Procedia*, vol. 83, pp. 624–633, Jan. 2016, doi: 10.1016/J.PHPRO.2016.08.065.
37. T. Fujieda *et al.*, "First demonstration of promising selective electron beam melting method for utilizing high-entropy alloys as engineering materials," *Mater Lett*, vol. 159, pp. 12–15, Nov. 2015, doi: 10.1016/J.MATLET.2015.06.046.
38. H. Shiratori *et al.*, "Relationship between the microstructure and mechanical properties of an equiatomic AlCoCrFeNi high-entropy alloy fabricated by selective electron beam melting," *Materials Science and Engineering: A*, vol. 656, pp. 39–46, Feb. 2016, doi: 10.1016/J.MSEA.2016.01.019.
39. T. Fujieda, H. Shiratori, K. Kuwabara, and T. Kato, "First demonstration of promising selective electron beam melting method for utilizing high-entropy alloys as engineering materials," *Mater Lett*, vol. 159, pp. 12–15, 2015, doi: 10.1016/j.matlet.2015.06.046.
40. T. Fujieda *et al.*, "CoCrFeNiTi-based high-entropy alloy with superior tensile strength and corrosion resistance achieved by a combination of additive manufacturing using selective electron beam melting and solution treatment," *Mater Lett*, vol. 189, pp. 148–151, Feb. 2017, doi: 10.1016/J.MATLET.2016.11.026.
41. Y. Brif, M. Thomas, and I. Todd, "The use of high-entropy alloys in additive manufacturing," *Scr Mater*, vol. 99, pp. 93–96, Apr. 2015, doi: 10.1016/J.SCRIPTAMAT.2014.11.037.

42. T. Fujieda, H. Shiratori, K. Kuwabara, M. Hirota, and T. Kato, "CoCrFeNiTi-based high-entropy alloy with superior tensile strength and corrosion resistance achieved by a combination of additive manufacturing using selective electron beam melting and solution treatment," *Mater Lett*, vol. 189, no. September 2016, pp. 148–151, 2017, doi: 10.1016/j.matlet.2016.11.026.
43. Z. G. Zhu *et al.*, "Selective laser melting enabling the hierarchically heterogeneous microstructure and excellent mechanical properties in an interstitial solute strengthened high entropy alloy," <http://mc.manuscriptcentral.com/tmrl>, vol. 7, no. 11, pp. 453–459, Nov. 2019, doi: 10.1080/21663831.2019.1650131.
44. J. G. Kim *et al.*, "Nano-scale solute heterogeneities in the ultrastrong selectively laser melted carbon-doped CoCrFeMnNi alloy," *Materials Science and Engineering: A*, vol. 773, p. 138726, Jan. 2020, doi: 10.1016/j.MSEA.2019.138726.
45. D. B. Miracle, "High entropy alloys as a bold step forward in alloy development," *Nat Commun*, vol. 10, no. 1, Dec. 2019, doi: 10.1038/S41467-019-09700-1.
46. J. M. Park *et al.*, "Superior tensile properties of 1%C-CoCrFeMnNi high-entropy alloy additively manufactured by selective laser melting," <http://mc.manuscriptcentral.com/tmrl>, vol. 8, no. 1, pp. 1–7, Jan. 2019, doi: 10.1080/21663831.2019.1638844.
47. R. Zhou *et al.*, "Microstructures and mechanical properties of C-containing FeCoCrNi high-entropy alloy fabricated by selective laser melting," *Intermetallics (Barking)*, vol. 94, pp. 165–171, Mar. 2018, doi: 10.1016/J.INTERMET.2018.01.002.
48. M. Song, R. Zhou, J. Gu, Z. Wang, S. Ni, and Y. Liu, "Nitrogen induced heterogeneous structures overcome strength-ductility trade-off in an additively manufactured high-entropy alloy," *Appl Mater Today*, vol. 18, p. 100498, Mar. 2020, doi: 10.1016/J.APMT.2019.100498.
49. H. Zhang, W. Wu, Y. He, M. Li, and S. Guo, "Formation of core-shell structure in high entropy alloy coating by laser cladding," *Appl Surf Sci*, vol. 363, pp. 543–547, Feb. 2016, doi: 10.1016/J.APSUSC.2015.12.059.
50. Y. He, J. Zhang, H. Zhang, and G. Song, "Effects of Different Levels of Boron on Microstructure and Hardness of CoCrFeNiAlxCu<sub>0.7</sub>Si<sub>0.1</sub>By High-Entropy Alloy Coatings by Laser Cladding," *Coatings 2017, Vol. 7, Page 7*, vol. 7, no. 1, p. 7, Jan. 2017, doi: 10.3390/COATINGS7010007.
51. A. Amar *et al.*, "Additive manufacturing of high-strength CrMnFeCoNi-based High Entropy Alloys with TiC addition," *Intermetallics (Barking)*, vol. 109, pp. 162–166, Jun. 2019, doi: 10.1016/J.INTERMET.2019.04.005.
52. J. Li *et al.*, "Additive manufacturing of high-strength CrMnFeCoNi high-entropy alloys-based composites with WC addition," *J Mater Sci Technol*, vol. 35, no. 11, pp. 2430–2434, Nov. 2019, doi: 10.1016/J.JMST.2019.05.062.
53. B. Li, L. Zhang, Y. Xu, Z. Liu, B. Qian, and F. Xuan, "Selective laser melting of CoCrFeNiMn high entropy alloy powder modified with nano-TiN particles for additive manufacturing and strength enhancement: Process, particle behavior and effects," *Powder Technol*, vol. 360, pp. 509–521, Jan. 2020, doi: 10.1016/J.POWTEC.2019.10.068.
54. P. F. Jiang, C. H. Zhang, C. L. Wu, S. Zhang, J. B. Zhang, and A. O. Abdullah, "Microstructure and Properties of CeO<sub>2</sub>-Modified FeCoCrAlNiTi High-Entropy Alloy Coatings by Laser Surface Alloying," *Journal of Materials Engineering and Performance 2020 29:2*, vol. 29, no. 2, pp. 1346–1355, Feb. 2020, doi: 10.1007/S11665-020-04621-3.
55. S. Chen, X. Chen, L. Wang, J. Liang, and C. Liu, "Laser cladding FeCrCoNiTiAl high entropy alloy coatings reinforced with self-generated TiC particles," *J Laser Appl*, vol. 29, no. 1, p. 012004, Nov. 2016, doi: 10.2351/1.4966052.
56. C. Kenel, N. P. M. Casati, and D. C. Dunand, "3D ink-extrusion additive manufacturing of CoCrFeNi high-entropy alloy micro-lattices," *Nat Commun*, vol. 10, no. 1, Dec. 2019, doi: 10.1038/S41467-019-08763-4.
57. J. U. Surjadi, L. Gao, K. Cao, R. Fan, and Y. Lu, "Mechanical Enhancement of Core-Shell Microlattices through High-Entropy Alloy Coating," *Scientific Reports 2018 8:1*, vol. 8, no. 1, pp. 1–10, Apr. 2018, doi: 10.1038/s41598-018-23857-7.
58. T. Wohlers, "Rapid Prototyping & Tooling State of the Industry Annual Worldwide Progress Report Rapid Prototyping & Tooling State of the Industry Annual Worldwide Progress Report TERRY WOHLERS 2 0 0 2".

59. J. P. Kruth, L. Froyen, J. van Vaerenbergh, P. Mercelis, M. Rombouts, and B. Lauwers, "Selective laser melting of iron-based powder," *J Mater Process Technol*, vol. 149, no. 1–3, pp. 616–622, Jun. 2004, doi: 10.1016/J.JMATPROTEC.2003.11.051.
60. X. P. Li, M. P. Roberts, S. O'Keeffe, and T. B. Sercombe, "Selective laser melting of Zr-based bulk metallic glasses: Processing, microstructure and mechanical properties," *Mater Des*, vol. 112, pp. 217–226, Dec. 2016, doi: 10.1016/J.MATDES.2016.09.071.
61. M. Saha, "A Brief Discussion on High-Entropy Alloys vs Compositionally Complex Alloys," Oct. 2021, doi: 10.20944/PREPRINTS202110.0075.V1.
62. Saha, M. (2022). Densification and characterization of pressureless sintered ZrB<sub>2</sub>-20 vol% MoSi<sub>2</sub> ultra high temperature ceramic composites. M. Mallik et al. *Densification and characterization of pressureless sintered ZrB<sub>2</sub>-20 vol% MoSi<sub>2</sub> ultra high temperature ceramic composites*, 47, 77-82.

**Disclaimer/Publisher's Note:** The statements, opinions and data contained in all publications are solely those of the individual author(s) and contributor(s) and not of MDPI and/or the editor(s). MDPI and/or the editor(s) disclaim responsibility for any injury to people or property resulting from any ideas, methods, instructions or products referred to in the content.